Microstructure and Properties of Sintered Tungsten Heavy Alloys

F.A. Khalid and M.R. Bhatti

(Submitted 10 August 1998; in revised form 4 September 1998)

The microstructure and properties of liquid-phase sintered tungsten heavy alloys were studied. The structure and segregation of the impurity elements at the interfacial boundaries were examined using scanning electron microscopy (SEM) and fine-probe energy dispersive spectroscopy (EDS) microanalysis. Test results of mechanical properties are presented and correlated with fracture behavior of the liquid-phase sintered tungsten alloys. It was found that the Fe-Ni-W alloy exhibits superior properties as compared with the Cu-Ni-W alloy. The detection of copper was found across tungsten grains and matrix that could be associated with inferior properties of the Cu-Ni-W alloy as compared to the Fe-Ni-W alloy. Although the fracture was predominantly brittle in both alloys, complex fracture modes seem to be operative due to the composite microstructure of the alloys. Evidence of microsegregation was observed that also contributed primarily to the brittle failure in the alloys. The impurity elements, such as sulfur and phosphorus, were detected at the tungsten matrix and tungsten-tungsten particle boundaries.

Keywords decohesion, dihedral angle, impurities, line-scan image, microsegregation, solubility, tungsten sintered alloys

1. Introduction

The tungsten heavy alloys are used in a wide range of applications, such as counterweights, inertial systems, radiation shields, heavy electrical contacts, and kinetic energy penetrators (Ref 1-4). They are made by the well-known liquid-phase sintering process, whereby maximum densification can be achieved. The alloy systems, such as Cu-Ni-W, Fe-Ni-W, Fe-Co-Ni-W, and Cu-W, contain about 80 to 98% tungsten, and consolidation occurs by dissolution of liquid phase and solid-solid contacts as a capillary force. The dimensional stability and nonuniformity in the properties observed frequently in sintered alloys can be controlled by optimization of the sintering process and elimination of impurity elements. Recently, improvement in the properties has been achieved through strain strengthening and subsequent heat treatment (Ref 5). However, variation in the properties and performance of sintered tungsten heavy alloys has been attributed to different processing conditions (Ref 6, 7).

In this work, the effect of microstructure on the mechanical properties of liquid-phase sintered heavy tungsten alloys has been studied. The influence of microsegregation observed in the tungsten matrix and tungsten-tungsten grain boundaries on the fracture behavior of the alloys is also examined.

2. Experimental Procedure

The liquid-phase sintered tungsten alloys were made using high purity elements. The chemical compositions of the experimental tungsten heavy alloys are presented in Table 1. The green compacts were formed by mechanical mixing and isostatic pressing of powders. The sintering was carried out at about 1500 °C under the reducing atmosphere of hydrogen. The specimens were prepared using standard metallographic techniques, and grain size was measured by the linear intercept method. The metal powders and sintered alloys were examined in a Philips XL 30 scanning electron microscope, and line-scan microanalysis was performed using Link-ISIS energy dispersive spectroscopy (EDS). Tensile and unnotched Charpy impact testing was carried out using the alloy samples in the as-sintered condition.

F.A. Khalid, GIK Institute of Engineering Sciences and Technology, Topi, NWFP, Pakistan; and **M.R. Bhatti,** POF, Wah, Pakistan.

3. Results and Discussion

Metal Powder Morphology. Figure 1 shows the particulate morphology of copper, iron, nickel, and tungsten powders used in the production of alloys 1 and 2. The average size of particles of metal powders is given in Fig. 2, and it can be noted that copper particles were coarser than other powders used in the alloys. The shape of nickel, copper, and iron particles was spherical as compared to an angular shape observed in the tungsten particles. The angular-shaped particles may have been produced as a consequence of crushing of pure tungsten. Earlier work (Ref 8) reports the effect of particle size of metal powders on the final grain size achieved during liquid-phase sintering.

Table 1 Chemical composition of tungsten heavy alloys

	Composition (nominal), wt%			
Alloy	**Ni**	**Cu**	**Fe**	**W**
1	9.40	4.70	…	bal
2	7.50	…	4.75	bal

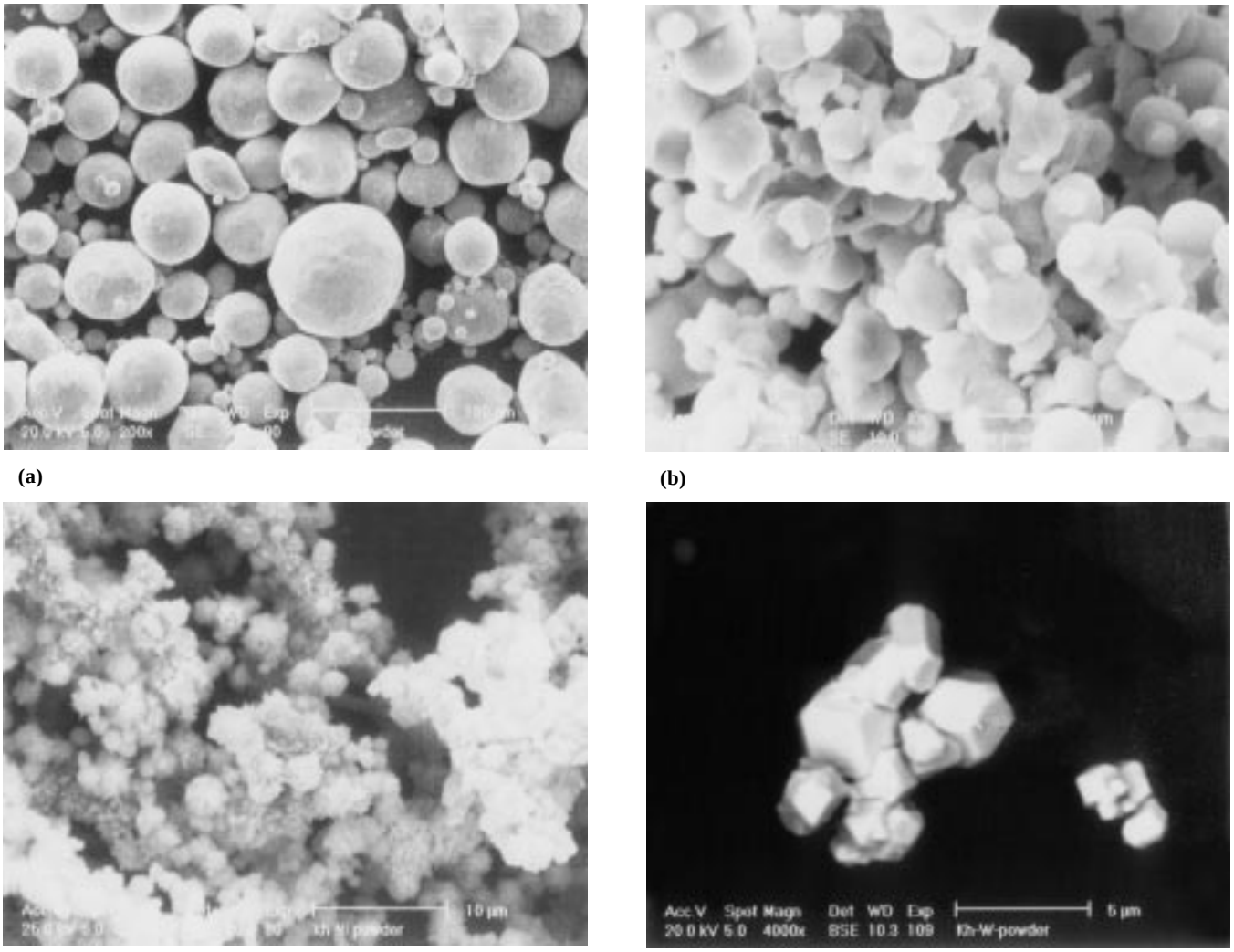

Fig. 1 Particulate morphology of metal powders: (a) copper, (b) iron, (c) nickel, and (d) tungsten

Sintered Microstructure. Figure 3 shows microstructures of liquid-phase sintered alloys 1 and 2. The tungsten grains can be found embedded in the liquid-phase copper-nickel and iron-nickel matrices, respectively. The average size of the tungsten grains in the alloys is given in Fig. 4. It can be noted that tungsten grains were finer and less densely packed in the microstructure of alloy 1 than alloy 2. Hence, a corresponding decrease in contiguity was observed in alloy 1 as compared to alloy 2, which is consistent with earlier studies (Ref 9).

Figure 5 shows EDS fine-probe microanalysis of the tungsten grains and liquid-phase matrices of alloys 1 and 2. The results agree with the solubility calculations of elements and Auger electron spectroscopic analysis reported by C. Lea et al. (Ref 1). The dihedral angle, connectivity, and contiguity parameters are controlled by the solid solubility of the elements in tungsten alloys as described in earlier studies (Ref 10, 11). The fine-probe analysis of tungsten grains showed no copper-nickel or iron-nickel concentration in the alloys as a consequence of a lack of solid solubility of these elements in tungsten.

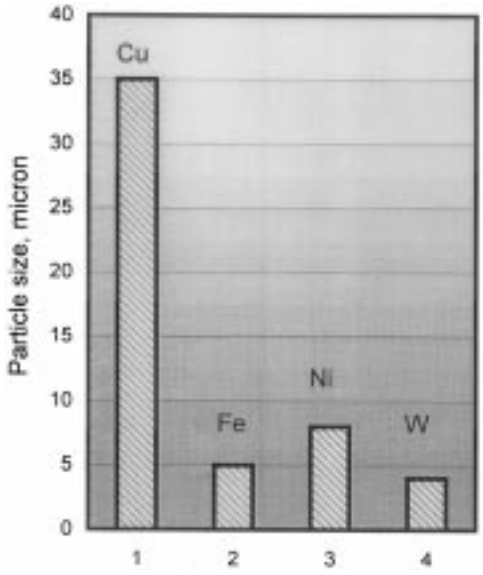

Fig. 2 Average particle size of metal powders

Mechanical Properties. Figure 6 shows tensile strength and impact toughness values measured in alloys 1 and 2. The tensile strength and impact toughness values decrease in alloy 1 as compared with alloy 2. The decrease in the tensile strength is consistent with contiguity in the case of alloy 1, but the variation in overall properties of both alloys may also be associated with the composition, fineness, and volume fraction of tungsten grains and microsegregation of impurity elements as described in the following paragraphs.

Fracture Behavior and Segregation. Figure 7(a-c) shows brittle fracture in the unnotched impact specimens of alloy 1. The cleavage fracture and facetting of tungsten grains are evident (Fig. 7b); however, the matrices failed in transgranular ductile mode, although the possibility of shear failure cannot be ruled out. Evidence of planar filamentary features at the tungsten-tungsten interfacial regions was also observed (Fig. 7c). Figure 8(a-c) reveals similar examples of brittle failure observed in alloy 2. However, the ductile failure along the region of tungsten grains was higher in alloy 1 than in alloy 2. Evidence of filamentary regions was also found due to poor wetting during sintering as reported elsewhere (Ref 6, 12, 13), which revealed a variation of matrix elements in the alloys. Figure 9 shows a schematic of possible fracture modes operative during impaction of the specimens. The fracture behavior observed in the specimens appeared to be consistent with earlier studies (Ref 6, 12).

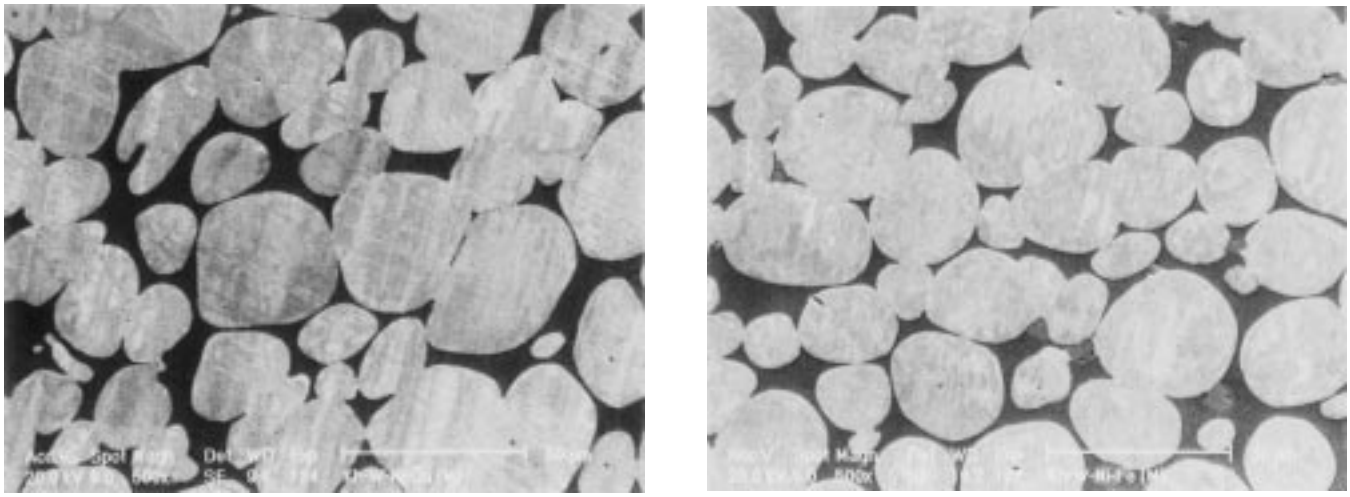

(a) **(b)**

Fig. 3 Microstructure of liquid-phase sintered (a) alloy 1 (Cu-Ni-W) and (b) alloy 2 (Fe-Ni-W)

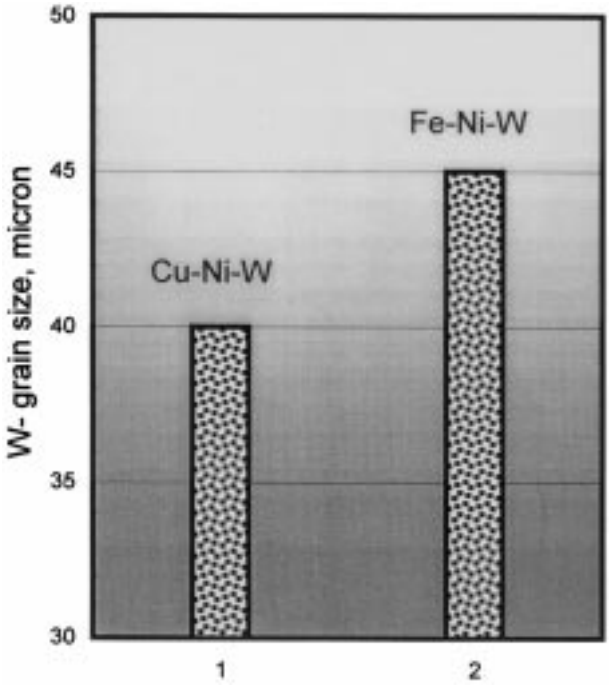

Fig. 4 Average tungsten grain size of alloys 1 and 2

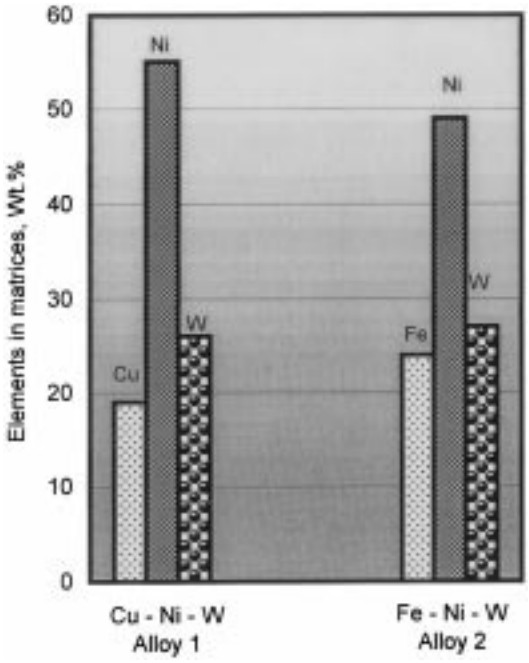

Fig. 5 EDS fine-probe microanalysis for matrices of alloys 1 and 2

Figure 10(a-b) shows SEM line-scan images and the concentration profiles of the elements from the fracture surfaces of both alloys. The microsegregation of sulfur and phosphorus at the planar facets of the tungsten grains was clearly evident in the alloys. The evidence of impurity elements at the grain boundaries is detrimental to and weakens the tungsten matrix and tungsten-tungsten boundary regions. The results are consistent with the observations on the effect of intrinsic structural parameters on the properties of tungsten alloys (Ref 11, 13). The concentration of copper at the fracture surface was uniform across the line scan in alloy 1 (Fig. 10a) unlike the peak of iron that was found only at the region of ductile matrix in alloy 2 (Fig. 10b). It is, however, likely that the presence of high concentration of copper across the microstructural phases led to greater degradation in the properties of alloy 1 than in alloy 2.

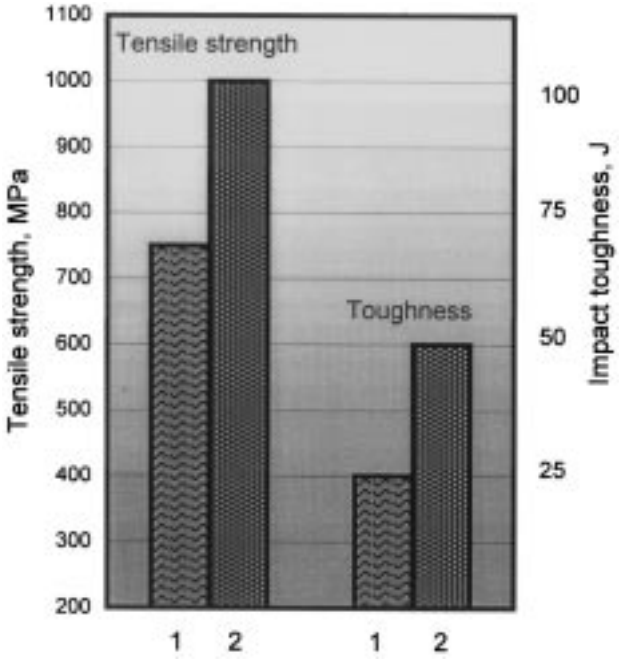

Fig. 6 Mechanical properties of alloys 1 and 2

4. Conclusions

- The particulate composite microstructure was observed in both tungsten alloys. The contiguity decreased with amount of tungsten in the alloys. The results showed no solid solubility of liquid phases in tungsten grains of the alloys.
- The mechanical properties were more inferior in alloy 1 than in alloy 2, which can be attributed primarily to the compositional effect, contiguity, and weaker bonding at the boundary regions due to impurity and segregation of matrix elements.
- Fractographic examination of both alloys revealed brittle failure and planar facetting of tungsten particles. Energy dispersive spectroscopy line-scan microanalysis of the

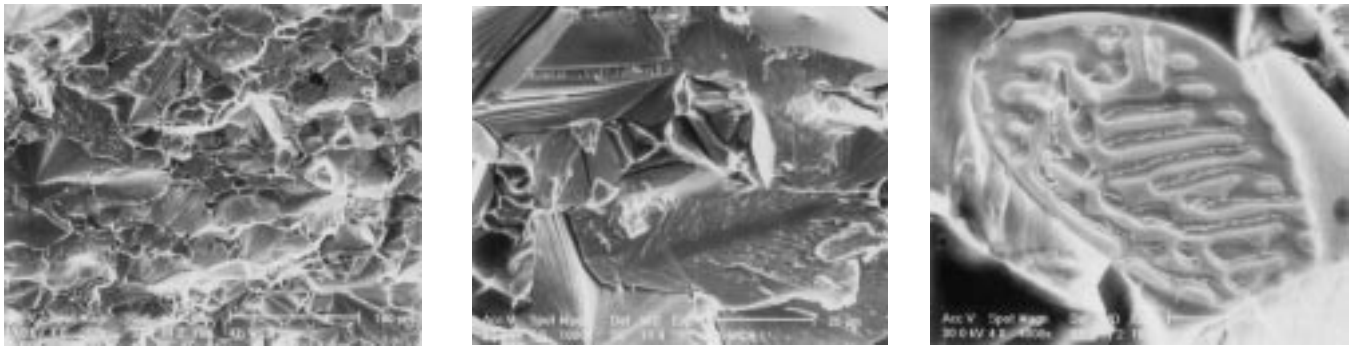

(a) **(b)** **(c)**

Fig. 7 SEM micrographs showing (a) brittle fracture, (b) cleavage facetting, and (c) planar filamentary features observed in alloy 1

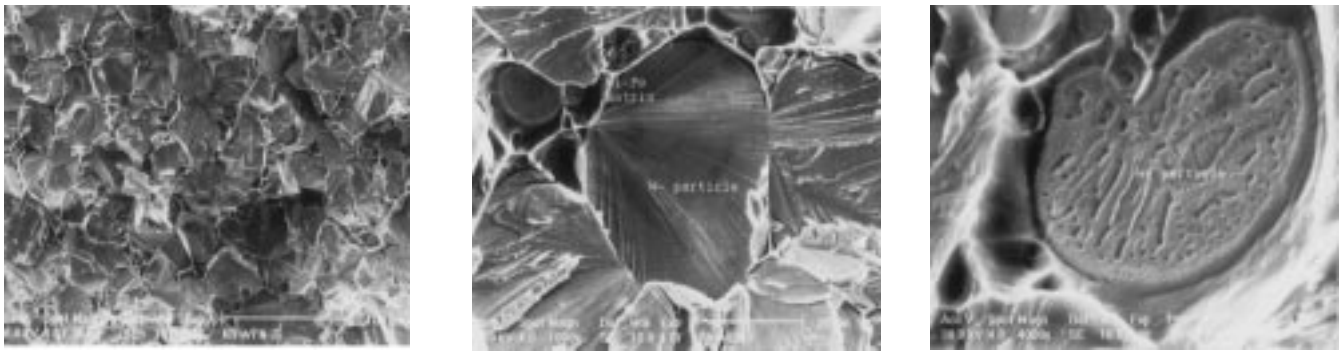

(a) **(b)** **(c)**

Fig. 8 SEM micrographs showing (a) brittle fracture, (b) cleavage facetting, and (c) planar filamentary features observed in alloy 2

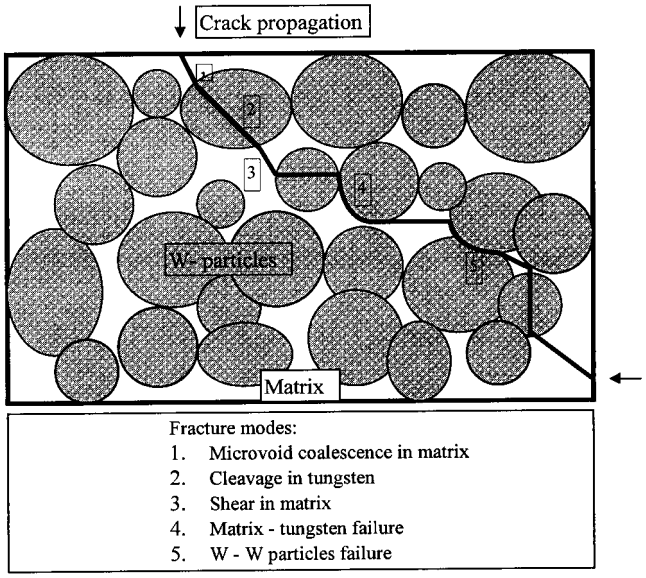

Fig. 9 Schematic of fracture modes in the tungsten alloys

fracture surfaces showed clearly the presence of sulfur and phosphorus impurity elements in addition to matrix elements contributing to decohesion of boundary regions as a result of partial wetting during the sintering process.

- The presence of copper throughout the line-scan microanalysis on the fracture surface in alloy 1 indicates segregation, which results in lower mechanical properties. Iron concentration was predominant only at the matrix region in alloy 2.

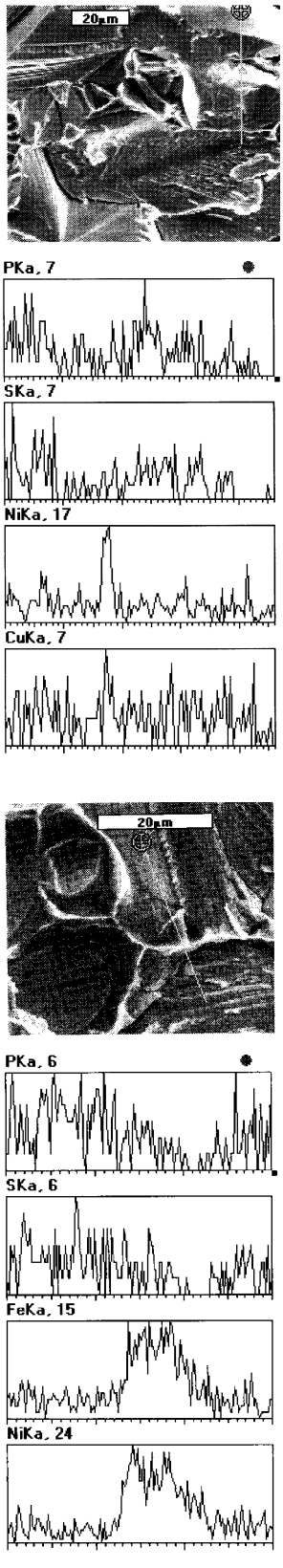

Fig. 10 SEM line-scan images and concentration profiles of impurity and matrices elements of (a) alloy 1 and (b) alloy 2

Acknowledgments

GIK Institute of Engineering Sciences and Technology is acknowledged for the provision of laboratory facilities, and POF is recognized for the provision of samples.

References

1. C. Lea, B.C. Muddle, and D.V. Edmonds, *Metall. Trans. A*, Vol 14, 1983, p 667
2. R.M. German, *Liqud Phase Sintering*, Plenum Press, 1985, p 228
3. V. Srikanth and G.S. Upadhaya, *Int. J. Refract. Hard Met.*, Vol 5, 1986, p 15
4. High Strain Rate Behavior of Refractory Metals and Alloys, Proc. Cincinnati, Ohio, TMS, 1991
5. G.X. Liang and E.D. Wang, *Mater. Sci. Technol.*, Vol 12, 1996, p 1032
6. D.V. Edmonds and P.J. Jones, *Metall. Trans. A*, Vol 10, 1979, p 289
7. A. Bose and R.M. German, *Metall. Trans. A*, Vol 19, 1984, p 2467
8. W.E. Lee and W.M. Rainforth, *Ceramic Microstructures*, Chapman and Hall, 1994, p 50
9. M.P. Seah and E.D. Hondros, *Int. Met. Rev.*, Vol 22, 1977, p 262
10. M.R. Eisenmann and R.M. German, *Int. J. Refract. Hard Met.*, Vol 3, 1984, p 1089
11. R.M. German, L.L. Bourguignon, and B.R. Rabin, *JOM*, Vol 37, 1985, p 36
12. M.P. Seah, *Acta Metall.*, Vol 28, 1980, p 955
13. F.A. Khalid and M.R. Bhatti, Advanced Materials, Processes, and Applications, *Proc. of EUROMAT '97*, FEMS, Maastricht, Netherlands, 1997